Two-color three pulse photon echo peak shift spectroscopy

Ritesh Agarwal, Bradley S. Prall, Abbas H. Rizvi, Mino Yang, and Graham R. Fleming

Citation: The Journal of Chemical Physics **116**, 6243 (2002); doi: 10.1063/1.1459414
View online: http://dx.doi.org/10.1063/1.1459414
View Table of Contents: http://scitation.aip.org/content/aip/journal/jcp/116/14?ver=pdfcov
Published by the AIP Publishing

Two-color three pulse photon echo peak shift spectroscopy

Ritesh Agarwal, Bradley S. Prall, Abbas H. Rizvi, Mino Yang, and Graham R. Fleming[a)]
Department of Chemistry, University of California, Berkeley and Physical Biosciences Division, Lawrence Berkeley National Laboratory, Berkeley, California 94720

(Received 29 October 2001; accepted 18 January 2002; publisher error corrected 1 November 2002)

Two-color three pulse photon echo peak shift spectroscopy (2C3PEPS) has been used to probe correlation in electronic transitions in two different regions of the electronic spectrum of a chromophore in the condensed phase. The 2C3PEPS can be done in an ''uphill'' or a ''downhill'' sense, where the first two interactions are of lower (higher) frequency than the final interaction with the radiation field. In both cases no correlation between the two spectral regions is observed at very short times. Different parts of the spectrum gain correlation owing to ultrafast solvent motion and the accompanying Stokes shift. We propose a model for the spectral shift that incorporates a conditional probability distribution for transition frequencies in the two spectral regions. The model qualitatively reproduces all the features of complete numerical simulations. Our results show that memory is partially conserved during the spectral diffusion process from the pump to the probe region. The downhill difference peak shift is very sensitive to the time scale of the inertial component of solvation and seems very promising for an accurate determination of this time scale.
 [DOI: 10.1063/1.1459414]

I. INTRODUCTION

Ultrafast resonant four-wave mixing spectroscopy has seen a steady development since the pioneering work of Yajima and co-workers,[1] and Weiner and Ippen.[2] In particular, various forms of photon echo spectroscopy including the three pulse photon echo peak shift (3PEPS),[3–7] time gated[8,9] and heterodyne detected photon echoes[10,11] have been demonstrated and applied to a variety of systems.[12,13] In this paper we describe a variant of the 3PEPS experiment in which one of the three input pulses is centered at a different frequency from the other two pulses—i.e., two-color 3PEPS (2C3PEPS). The experiment was first proposed by Yang and Fleming as a probe for electronic mixing in molecular complexes,[14] however, in the present work we simply select both colors to lie within the bandwidth of the broad electronic absorption band of dilute solutions of dye molecules.

In order to simplify the experimental arrangement the two colors were selected by filtering a single 15 fs (bandwidth$\sim$70 nm FWHM) pulse from a cavity-dumped Ti:sapphire oscillator. It might be supposed that carrying out a peak shift measurement with ''two pieces'' of a pulse would yield identical information to that obtained with the entire pulse. In principle, this must be so, but in practice when all three pulses are identical the four-wave mixing signal is dominated by degenerate or nearly degenerate processes, and the contribution of events in which the third interaction takes place at a significantly different frequency from the first two is quite small. The two-color experiment projects out this nondegenerate or ''off-diagonal'' contribution and in doing so has the potential to reveal new information on the system dynamics. Perhaps the most evident type of new information is the ability to observe dynamics on different regions of the potential surface, perhaps even to map the entire surface, rather than simply describing the disappearance of the initially created population. In addition, because the peak shift method is sensitive to the degree of memory of the transition frequency of the system,[3–5,7] the two-color experiment contains unique information of the correlation in transition frequencies between initial and final states.

It is evident that the two-color experiments cannot be treated in the ''impulsive'' limit where the excitation pulses are considered of vanishing duration. This means that particular care must be paid to the influence of finite pulse duration, especially during the region of pulse overlap, where pulse ordering cannot be enforced. We have found that the information present in 2C3PEPS can be most readily appreciated by defining and measuring two different types of peak shift via two different delay-scanning procedures. We refer to these as type I and type II scans, giving rise to peak shifts defined as τ_{I}^{*} and τ_{II}^{*}, respectively, definitions of which will be discussed in Sec. II. The type I scan is that used previously for 3PEPS measurements,[3,7] while type II, as will be explained below, corresponds to a nonrephasing or free-induction decay (FID) sequence. The difference peak shift, $\Delta\tau^{*}=\tau_{\mathrm{I}}^{*}-\tau_{\mathrm{II}}^{*}$, is a useful quantity that minimizes the influence of finite pulse duration and will be discussed in some detail below.

II. EXPERIMENTAL METHOD

Two-color three pulse photon echo experiments were performed by using the output of a home-built, cavity dumped Ti:sapphire laser that produced 15 fs (FWHM, E-squared) pulses at a repetition rate of 250 kHz. The spectral width of these 15 fs pulses was $\sim$70 nm (FWHM). The

a)Electronic mail: grfleming@lbl.gov

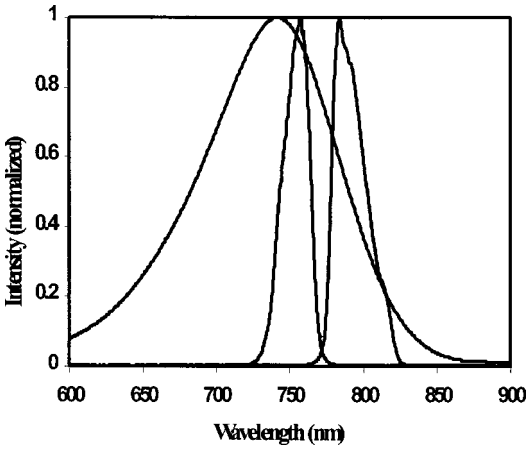

FIG. 1. The absorption spectrum of the dye IR144 in methanol. Also shown are the spectra of the excitation pulses centered at 750 and 800 nm.

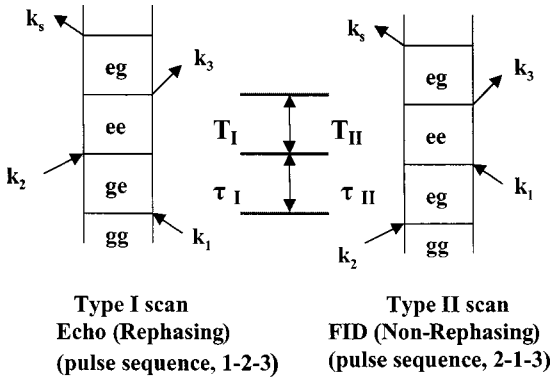

FIG. 2. The Feynman diagrams for the echo and FID pathway for the signal in $\mathbf{k}_3+\mathbf{k}_2-\mathbf{k}_1$ phase matched direction.

two-color photon echo interferometer is the same as described previously for one-color echo experiments.[3] In short, the pulses were split into three beams of roughly equal intensities and arranged in an equilateral triangle geometry. In the two-color experiment, the first two interactions are from spectrally identical pulses and the third interaction is from a spectrally distinct pulse. The two different colors for our experiment were generated by placing interference filters (Corion, 750 ± 20 nm, 800 ± 20 nm) in each of the arms. Since the interference filters change the beam path slightly, great care was taken to ensure that the three beams of the interferometer were collinear and had minimum deviation with respect to each other. The spectrally filtered pulses were of ~42–45 fs (FWHM, *E*-squared) duration and the pulse energy at the sample was ~200 pJ per pulse. Due to the spectral filtering process, all the pulses had a minor (~10% amplitude, 120 fs) exponential tail. The sample (the dye IR144 in methanol) was flowed in a 100 μm quartz cell to minimize thermal effects on the measured signal.

Figure 1 shows the spectra of the two pulses along with the absorption spectrum of IR144 in methanol. In a three pulse photon echo experiment, the system interacts with three pulses, with momentum vectors, k_1, k_2, and k_3, respectively. When we write k_1, k_2, or k_3 we shall imply only the momentum of the pulses (direction of the propagation of beams) and not their actual interaction sequence with the sample. A key aspect of the peak shift method is the distinction between rephasing and nonrephasing pulse sequences, as depicted in the two Feynman diagrams of Fig. 2. There are three time periods in each diagram; an initial coherence, a population, and a final coherence period. In the left-hand diagram the phase of the second coherence is the complex conjugate of the first coherence and rephasing (echo generation) can occur if and only if the system has rephasing capability. In the right-hand diagram the two coherence periods have the same phase and, in contrast with the left-hand diagram, only free induction decay is possible, regardless of the rephasing capability of a system. Therefore the signals generated by the two types of scans should have distinct characteristics when the system has rephasing capability. Note that the difference between the two, provided that pulse 3 is constrained to interact last, is simply the ordering of pulses 1 and 2. In a standard 3PEPS experiment, the time integrated echo profiles are measured as a function of the coherence period (pulses 1 and 2), for fixed values of the population period (pulses 2 and 3). The echo peak shifts obtained from the echo profiles are recorded as a function of the population period. The type I peak shift is the same as the standard 3PEPS described above, i.e., for the pulse sequence, 1–2–3. The time between pulse 1 and 2 is called the coherence time (τ_{I}), and between pulses 2 and 3 is called the population period (T_{I}). The peak shift for this type of scan is denoted as $\tau_{\mathrm{I}}^*(T_{\mathrm{I}})$.

The type II peak shift is obtained from the pulse sequence 2–1–3. From Fig. 2 it is clear that this pulse ordering corresponds to the FID diagram for the $k_3+k_2-k_1$ phase matching direction. In this type of scan, the time between pulses 2 and 1 is called τ_{II} (a positive value of τ_{II} corresponds to pulse 2 interacting before pulse 1). The population period, T_{II}, is determined between pulses 1 and 3 and the peak shift obtained by this procedure (type II scan) is denoted as $\tau_{\mathrm{II}}^*(T_{\mathrm{II}})$. After the peak shifts for both types of scanning methods are measured, the difference peak shift (DPS) as a function of time T can then be defined as $\Delta\tau^*(T)=\tau_{\mathrm{I}}^*(T_{\mathrm{I}}=T)-\tau_{\mathrm{II}}^*(T_{\mathrm{II}}=T)$. When a system has no rephasing capability, both types of scans will generate signals containing the same information (FID). In this case, the experimental observables (τ_{I}^* and τ_{II}^*) should be identical and consequently $\Delta\tau^*=0$. Otherwise we expect a distinction between the signals generated by the two types of scanning methods and thus a nonzero value of $\Delta\tau^*$. In this paper we introduce $\Delta\tau^*$ as a measure of the rephasing capability of a system. One advantage of $\Delta\tau^*$ in measuring the rephasing capability over the peak shift itself will be discussed in Sec. V.

III. RESULTS

Two-color echo profiles for both type I and type II scans are shown in Fig. 3. For population time, $T=0$ fs, the two scans produce nearly identical results, with both profiles peaking at a coherence time of 12 fs. The two profiles were recorded simultaneously in the two different phase matched directions and were normalized to account for different detector sensitivities. This normalization is not required if the

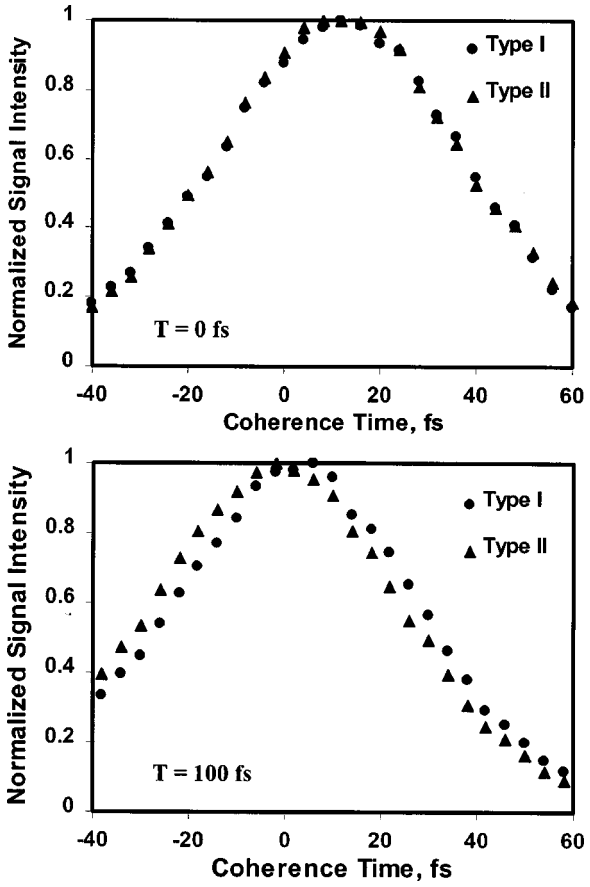

FIG. 3. Experimental two-color echo profiles (750–750–800 nm) for both type I and II scans for IR144 in methanol. Top figure: population time, $T=0$ fs. Bottom figure: population time, $T=100$ fs.

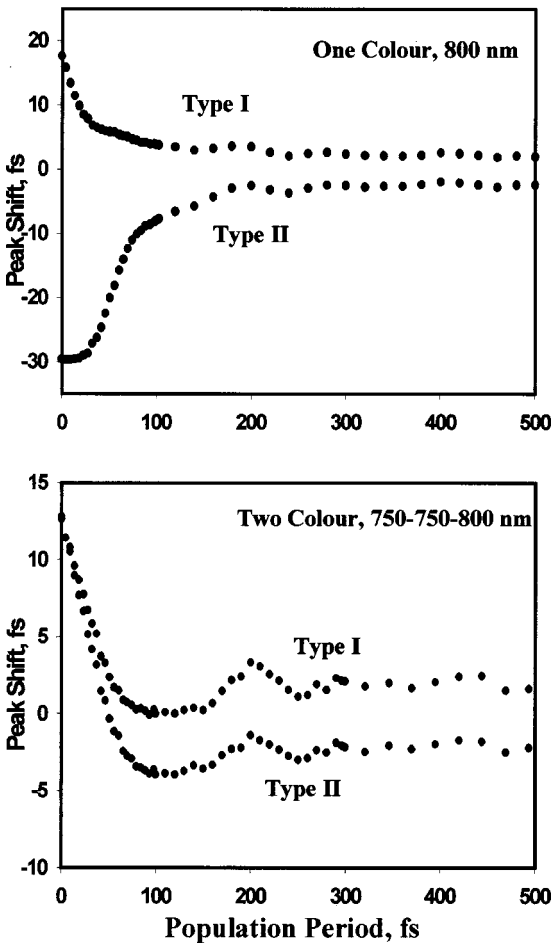

FIG. 4. Top figure: the type I and II peak shift data for the one-color (800 nm), and bottom figure: the two-color (750–750–800 nm) case for IR 144 in methanol. Also shown is the difference peak shift for the downhill (750–750–800 nm) and the uphill (800–800–750 nm) case.

profiles are recorded in successive scans in the same phased matched direction and hence on the same detector. For population time, $T=100$ fs, the two scans produce slightly different results with the type I peaking near zero coherence and the type II peaking at negative coherence time. The experimental data for type I and II peak shifts for both one- and two-color cases are shown in Fig. 4. We have not shown the echo profiles for the two-color experiment at different population periods, as they look very similar to the profiles obtained from the one-color experiment. The peak shift values (for both one- and two-color experiments) are determined from the maximum value obtained after fitting the individual experimental echo profiles with a single Gaussian function. For one-color experiments, the type I peak shift is identical to that previously reported for IR144 in methanol.[3] The type II peak shift starts at a large negative value, indicating a strong preference for the system to generate an echo signal. The negative values of type II peak shifts imply a pulse ordering of 1–2–3 and hence generates an echo signal (Fig. 2). The type II peak shift scan for one color does not carry any information that is significantly different from the type I scan and hence will not be discussed. Before we discuss the two-color results, we introduce the concept of ''downhill'' (e.g., 750–750–800 nm) and ''uphill'' (e.g., 800–800–750 nm) difference peak shifts. The results for the two-color peak shift are very interesting and shown in the lower panel of Fig. 4. Both the type I and II peak shifts for uphill and downhill cases start at approximately the *same positive* value. The echo profiles are the same irrespective of the pulse ordering 1–2–3 or 2–1–3, which strongly suggests, based on the argument in Sec. II, that no rephasing capability is observed at time zero and thus the system does not generate any echo signal. The corresponding difference peak shift data obtained from type I and II peak shifts are shown in Fig. 5 for uphill and downhill two-color cases. In both cases the signal rises from near zero to a maximum and decays on a much longer time scale back to zero.

IV. NUMERICAL SIMULATIONS

In order to investigate the information content of the two-color peak shift, in particular the difference peak shift, we carried out numerical simulations of the signals. Nonlinear optical response functions for dilute solutions of chromophores can be described via the transition frequency correlation function. This correlation function, $M(t)$, is often modeled as a sum of a Gaussian, exponential, and damped cosine components representing the inertial and diffusive solvation responses, and the intramolecular vibrational modes, respectively. The $M(t)$ is used to calculate the line

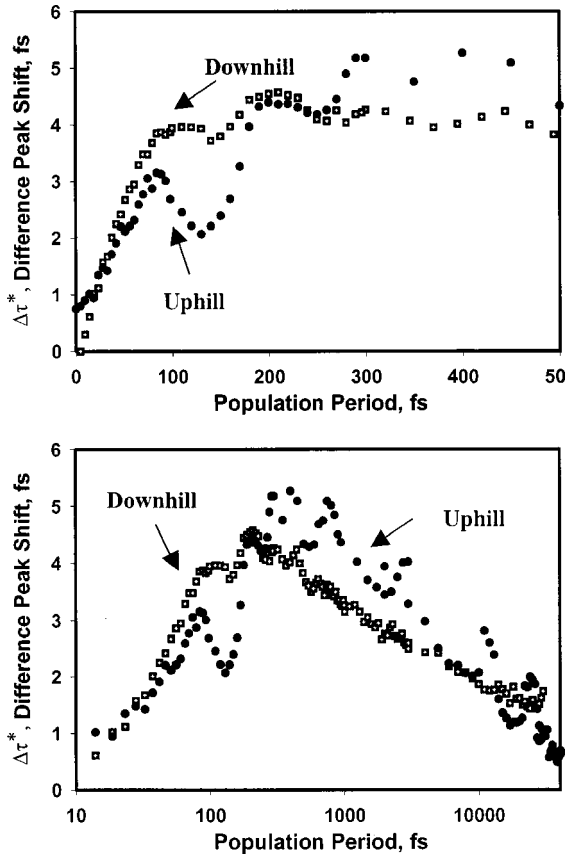

FIG. 5. Difference peak shift for two color (750–750–800 nm) as obtained from Fig. 4. The bottom figure shows the same data on a logarithmic scale for the population period.

broadening function, $g(t)$, which in turn is used to calculate the various optical signals.[15] The different frequencies of the laser pulses for the two-color experiment are incorporated via the expression for the electric field of the pulses.

In a population-sensitive technique such as the transient grating (2CTG) method, a significant contribution to the two-color signal would be expected to arise from population transfer (for example, wave packet motion) from the "excited" to the "probed" region. In these dilute systems the four-wave mixing signal must involve all four field interactions with the same molecule, and the initial amplitude of, for example, a 2CTG signal is measured and calculated to be quite small (~10%) compared to the one-color signal. Both numerical and analytical models for the two-color transient grating experiment will be described in a separate publication and we now focus on the two-color peak shift for the remainder of the paper.

The molecular mechanisms behind the rise and decay of the difference peak shift from its near zero initial value are of particular interest. Figure 6 presents the results of simulations using three different models: (i) The single-stick model—namely, a two-level electronic system linearly coupled to a solvent bath. The transition frequency correlation function is given by a single Gaussian component. (ii) The two-stick model, obtained by adding one intramolecular vibration, $\hbar\omega = 500\ \mathrm{cm}^{-1}$, $\lambda = 75\ \mathrm{cm}^{-1}$ to model (i), and (iii) a many-mode model, in which a large number (in this case 35) of intramolecular modes are added to model (i). The calculations are carried out at 300 K. The simulations are done for the downhill case and incorporate finite duration pulses. For model (i), the initial difference peak shift starts near zero and increases to a maximum value. For model (ii), the difference peak shift does not start from zero, showing clearly that such a model cannot describe data such as those in Fig. 5. The difference peak shift for model (iii) starts at a value that is very close to zero, and hence resembles our experimental data in this regard.

Perhaps the most striking aspect of the experimental data is the rise in the difference peak shift to a maximum, followed by a rather slow decay to zero. A progressively increasing distinction between τ_{I}^* and τ_{II}^* implies an apparent increase in the rephasing capability with an increasing population period. Eventually, however, all memory is lost and τ_{I}^* and τ_{II}^* again become identical. In Fig. 7 we show calculated downhill difference peak shifts for the (over) simple case when the transition frequency correlation function, $M(t)$, is given by a single Gaussian process; $M(t) = \lambda \exp(-t/\tau_g)^2$, where λ is the reorganization energy. Clearly the rise time of the $\Delta\tau^*$ is well correlated with the Gaussian time constant in the bath response, and the empirical expression, $T_{\max} \sim \tau_g[c_1 \Delta\omega \log(c_2/\lambda) + c_3]$, where $\Delta\omega$ is the frequency difference between the pulses and the c's are constants, describes the position of the maximum in $\Delta\tau^*$ quite well. The expres-

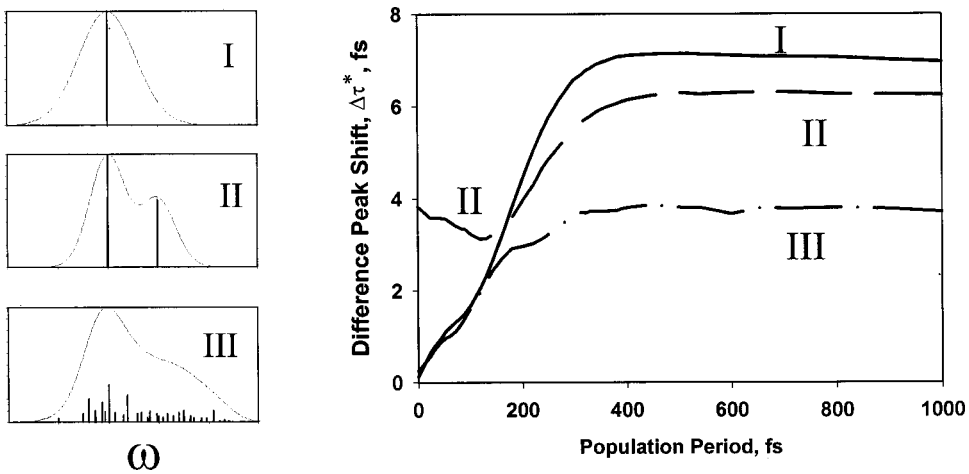

FIG. 6. The difference peak shift obtained from (i)–(iii) models. Refer to the text for details.

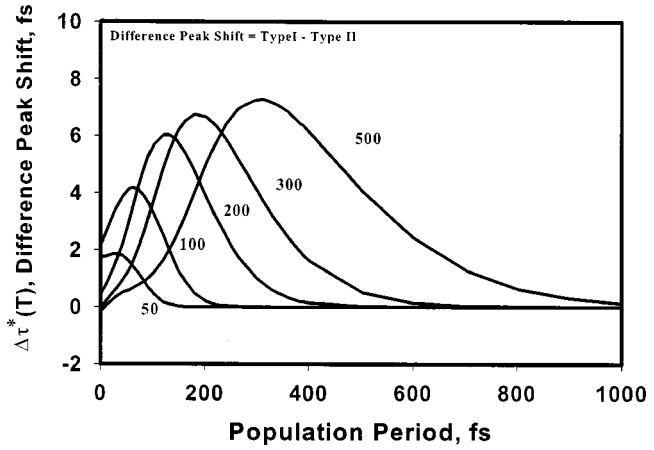

FIG. 7. Model calculations for the difference peak shift for the downhill case. The $M(t)$ consists of a single Gaussian ($\lambda = 600\ \mathrm{cm}^{-1}$) mode with varying time constant. The maximum value of the difference peak shift is clearly correlated with the Gaussian time constant.

sion was obtained empirically after performing extensive numerical simulations to characterize the dependence of the maximum of $\Delta\tau^*$ on the various parameters and is not a highly accurate formula. We found that the maximum of $\Delta\tau^*$ did not change appreciably on adding exponential components and a large number of intramolecular modes. This feature is very helpful in the accurate determination of the time scale of the ultrafast Gaussian component, which otherwise is difficult to obtain from one-color experiments in large measure because of the destructive interference from the intramolecular modes.[16]

In Fig. 8 we show simulated difference peak shifts for both downhill and uphill cases with a more detailed model for $M(t)$ that also includes two exponential components ($\lambda_1 = 75\ \mathrm{cm}^{-1}, \lambda_2 = 70\ \mathrm{cm}^{-1}, \tau_1 = 2500$ fs, $\tau_2 = 9000$ fs) and 35 intramolecular modes (see the figure caption). The simulations are shown for different values of the Gaussian time constant while keeping the rest of the parameters fixed. The rise in the downhill difference peak shift is not greatly influenced by the intramolecular contribution, aside from the superimposed oscillatory structure and remains well correlated with the Gaussian time scale, τ_g. The uphill difference peak shift, however, scarcely depends on the Gaussian time scale. Also note that the vibrational structure appears very different in the uphill and the downhill simulations, as it does also in the experimental data. Further, in the absence of the intramolecular vibrational contribution to $M(t)$, the uphill peak shift *is* sensitive to τ_g, and this sensitivity is apparently destroyed by the intramolecular vibrational contribution to the response.

V. DISCUSSION

Based on the numerical simulations described above, we now attempt to provide some physical insight into the form of the two-color difference peak shift, $\Delta\tau^*$.

Implicit in our model is the assumption that the spectral density is the same for each member of the ensemble. By this assumption each member of the ensemble can absorb over a range of different frequencies. Such a picture has been discussed, for example, in the context of instantaneous normal mode (INM) theory.[17–21] At very short times, the dynamics in liquids can be represented in terms of uncoupled harmonic modes that arise from collective motions of several solvent molecules.[17–21] The INM spectral densities and the solvation spectrum obtained by these methods typically reveal a broad distribution of solvent modes, and the spectral density can be further decomposed into different types of solvent motions (translation, libration, vibration, etc.).[17,18] Electronic transitions are coupled to these solvent modes. We now define two different mechanisms of line broadening. One is the homogeneous broadening that appears due to the vibronic transitions from a particular phonon state in the ground electronic state. This broad distribution of nuclear transitions as well as spectral evolution within the pulse duration accounts for the existence of a two-color four wave-mixing signal at short times. The other broadening mechanism is due to a distribution of the phonon occupation owing to thermal energy over the molecules in the ensemble, and is termed inhomogeneous broadening.

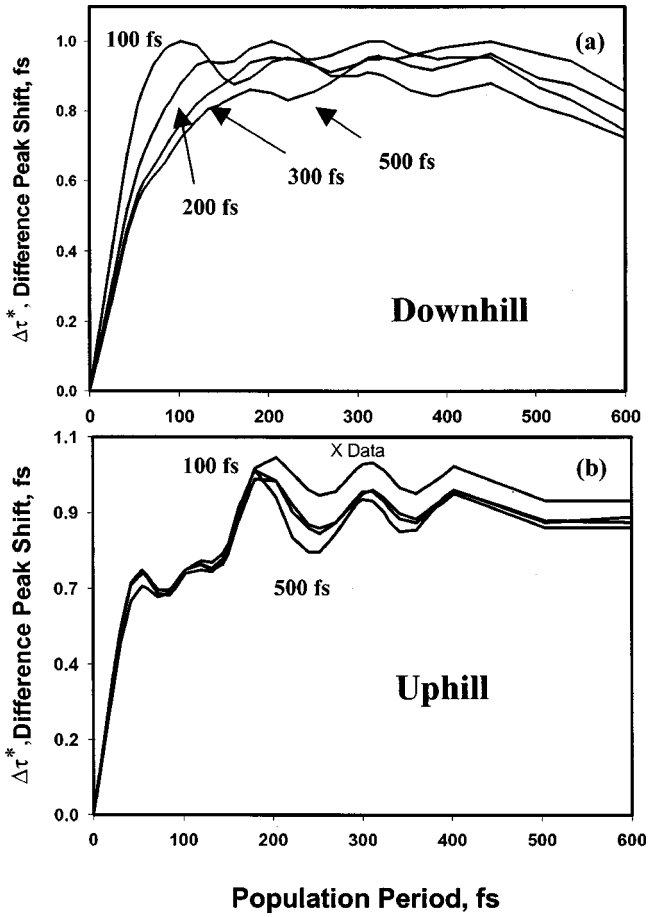

FIG. 8. Simulations for the downhill (top figure) and uphill (bottom figure) difference peak shift for different values of the Gaussian time constant. The plots are normalized to facilitate a direct comparison. The $M(t)$ consists of a Gaussian ($\lambda = 150\ \mathrm{cm}^{-1}$) with a varying time constant, and two exponential components ($\lambda_1 = 75\ \mathrm{cm}^{-1}$, $\lambda_2 = 70\ \mathrm{cm}^{-1}$, $\tau_1 = 2500$ fs, $\tau_2 = 9000$ fs) and 35 intramolecular modes with frequencies ranging from 150 to 1400 cm^{-1}. The total reorganization energy used for the intramolecular modes is 400 cm^{-1}. The center wavelengths of the excitation pulses are set at 750 and 800 nm.

As the simulations in Fig. 6 show, the initial difference

peak shift is zero for models (i) and (iii). The zero difference peak shift is obtained because the initial signals produced by type I and type II scans generate the same nonzero value for the initial peak shift. We discussed in Sec. II that the existence of a rephasing capability in a system will generate different values of the peak shift in the two types of scans. Thus, the zero initial difference peak shift obtained in the simulations implies that the model systems do not have any rephasing capability at short time. At first glance, this conclusion seems to contradict the observation of a finite value of the peak shift in each scan since it has been accepted that normal peak shift data is proportional to the rephasing capability of the system. However, this is not rigorously true at a very short population time, where the effect of pulse overlap is important.

In order to make clear what we mean by the pulse overlap effect, we illustrate the dependence of the convolution volume, which is derived from a perturbation theory treatment with respect to the electric field, on the experimental time variables (τ and T). In the type I scan, the third-order polarization is given by the sum of the following four contributions:

$$P_1(t)=\int_{-\infty}^{t}dt_3\int_{-\infty}^{t_3}dt_2\int_{-\infty}^{t_2}dt_1\,R_1(t,t_3t_2t_1)\times E(t_3)E(T+t_2)E(\tau+T+t_1),$$

$$P_2(t)=\int_{-\infty}^{t}dt_2\int_{-\infty}^{t_2}dt_3\int_{-\infty}^{t_3}dt_1\,R_2(t,t_3t_2t_1)\times E(t_3)E(T+t_2)E(\tau+T+t_1),$$

$$P_3(t)=\int_{-\infty}^{t}dt_3\int_{-\infty}^{t_3}dt_1\int_{-\infty}^{t_1}dt_2\,R_3(t,t_3t_2t_1)\times E(t_3)E(T+t_2)E(\tau+T+t_1),$$

$$P_4(t)=\int_{-\infty}^{t}dt_2\int_{-\infty}^{t_2}dt_1\int_{-\infty}^{t_1}dt_3\,R_4(t,t_3t_2t_1)\times E(t_3)E(T+t_2)E(\tau+T+t_1),$$

where $E(t)$ is a real envelope function of the electric field centered at $t=0$ and dynamical information on the nuclear motion and the energy detuning factors of the electric fields are described by the response functions, R_1-R_4. Detailed expressions for the response functions are irrelevant to the present discussion and can be found in Ref. 15. These equations describe a subset of the third-order polarization selected by the rotating wave approximation. As a result of this approximation, the volume of space subject to the time integral for the nonlinear polarization has become dependent on the experimental time variables, τ and T. As these equations show, the nonlinear polarization is given by a convolution integral with the response function including information on the nuclear dynamics and the envelope of electric fields over the subspace of time integral variables selected by the rotating wave approximation.

In Fig. 9, we illustrate the dependence of the volume of the subspace (weighted by the envelope function) on τ and T, which is calculated numerically from the above equations.

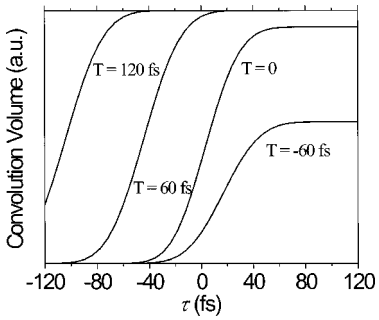

FIG. 9. Convolution volume for the third-order polarization as a function of the time delay between the first and second pulse (τ) for four different values of the time delay between the second and third pulse (T), which are denoted on each curve. A Gaussian envelope function with a FWHM of 48 fs is employed.

We set $R=$const and Gaussian envelope functions with a FWHM of 48 fs are employed for the light fields. As one can see, for short population times (T), the integral volume is strongly dependent on coherence time (τ) over an experimentally relevant range (about -40 to 40 fs). Therefore, a crucial factor determining the nature of nonlinear polarization at small values of T is the pulse overlap effect in addition to the fast nuclear dynamics. For example, if one tried to get peak shift data from this simple system with $R=$const (with no rephasing capability), a large positive value of an initial peak shift would be obtained since the signal intensity is proportional to the convolution volume. This is why we obtained a nonzero initial peak shift in the individual scans for the models (i) and (iii) but zero difference peak shift (reflecting no rephasing capability). This illustration shows that care is required in the interpretation of nuclear dynamics at short times probed by the conventional peak shift method. Following this argument, in order to extract the short time solvation dynamics, we need to remove the pulse overlap effect and we suggest that the difference peak shift method should be a powerful technique for this purpose.

The pulse overlap effect appears in both one- and two-color experiments at short times. However, since in a one-color experiment the system has a strong rephasing capability at short population periods, the type I and II peak shifts produce very different results, showing that the role of nuclear dynamics (rephasing capability) dominates over the pulse overlap effects in this case. However, at very long population times, the system loses its rephasing capability due to the dynamical processes and, as we can see in Fig. 9, the pulse overlap effect disappears as well. Therefore we expect the peak shift of the individual scans as well as the difference peak shift should be zero.

Based on the above discussion and the observation of a zero initial difference peak shift, for a two-color experiment, there is little or no rephasing capability at very short times and therefore the total signal is dominated by a FID signal. Since the effect of pulse overlap is the same for the type I and II peak shifts, the presence of a signal predominantly arising from FID (which will yield the same response function for the two scanning methods) gives rise to similar but finite values of type I and II peak shifts due to the pulse

overlap effect, as discussed above, and hence a zero value of a difference peak shift. Therefore, we have observed that the presence of a finite value of the peak shift itself at very short population periods may not imply that the system has a rephasing capability, and the difference peak shift method is more sensitive to the rephasing capability of the system.

The absence of a rephasing capability at very short times can also be understood from the instantaneous normal mode (INM) representation of liquids.[17] As a result of the two line broadening mechanisms, each line in the absorption spectrum is composed of transitions involving some linear combination (e.g., sum or difference frequency) of the solvent modes. Each solvent mode is coupled to the electronic transition with a particular coupling strength. Since a large number of solvent modes couple to the electronic transition, the coupling strength of each mode is generally small. Therefore, the probability of the same mode to appear both in the pump and probe regions via a long Franck–Condon progression is small. In other words, the pump pulse will excite a different set of transitions in the ensemble as compared to the probe (third) pulse. Since different parts of the spectrum may arise from completely different modes of the solvent, they are uncorrelated at short times, resulting in a free induction decay component to the signal. In model (ii) the initial difference peak shift is not zero because of the presence of a high-frequency intramolecular mode dressed with the same spectral density. Hence, the information of nuclear states at short times is already mixed between the transitions at different parts of the spectrum leading to nonzero values of the difference peak shift. As we add a large number of intramolecular modes, each dressed with the same spectral density, the difference peak shift again starts with a value close to zero. Adding a large number of intramolecular modes leads to transitions that also correspond to overtones, sums and difference frequencies of these fundamental modes[16] thereby creating another quasicontinuum of lines in the spectrum of electronic transitions. The effect of this second level of transitions corresponding to intramolecular modes is similar to the effect of a quasicontinuum of intermolecular modes. Transitions at two different parts of the spectrum again lose correlation at short times since they correspond to sets of transitions arising from completely different modes, in this case different solute modes.

As time goes on, the nuclear wave packet created in a nonequilibrium state evolves under the potential energy surface of the excited (ground) electronic state. This evolution of the wave packet leads to the Stokes shift and fluctuations in the electronic transition energy. As a result, a subset of the ensemble created by the initial pump frequency will move to a nuclear configuration corresponding to the electronic transition energy associated with the probe window, which means that the signal intensity should increase with time. Population-based two-color experiments will be sensitive only to the time dependence of the spectral shift, but it is difficult to extract details of the dynamics occurring during the spectral shift from these experiments.

The spectral shift is illustrated in panel (a) of Fig. 10, which serves to define the location of the pump (pulses 1 and 2) and probe (pulse 3) frequencies. Two extreme scenarios

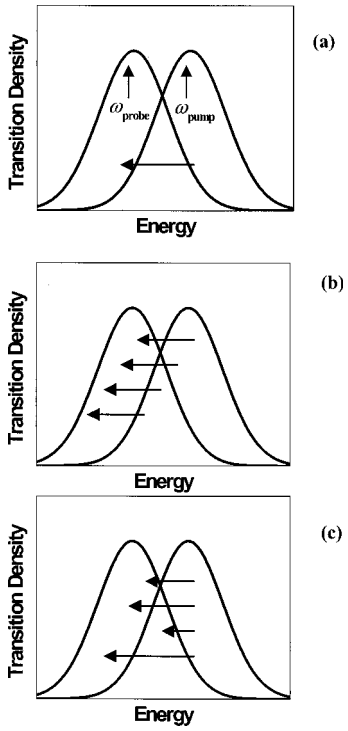

FIG. 10. The model for the time-dependent spectral shift. The panel (a) shows the spectral distribution at the pump and probe wavelengths. The panel (b) corresponds to the "rigid" case, where no memory is lost, i.e., no scrambling of transition frequencies occurs during the shift. The panel (c) depicts another extreme scenario where all the memory is lost, i.e., complete scrambling takes place during the shift.

for the spectral shift process can be envisaged. In one, the shift occurs in a "rigid" sense in which the relative position with respect to the mean frequency of the spectral band is conserved [panel (b) of Fig. 10]. In other words, a specific initial frequency gives rise to a specific final frequency. In the other mechanism, the probability for a given initial frequency to give a specific final frequency is independent of the final frequency, i.e., the shift randomizes the position within the band [panel (c)]. In a real spectral shift, both processes will coexist.

In order to create a physical picture for the phenomena underlying the two-color difference peak shift data, we present a simple analysis based on the assumption that the line broadening comes from a purely statistical distribution of transition energies in which each molecule has a unique transition energy (without the homogeneous broadening mentioned above). Noting that the rephasing capability is directly correlated with the fraction of the ensemble that conserves its transition energy, we examine the following time correlation function in which the fluctuation dynamics of the inhomogeneous distribution of transition energies is described by a conditional probability:

$$\langle \delta\epsilon_{pr}(t)\,\delta\epsilon_{pu}\rangle_{\mathrm{inhom}} = \frac{1}{N(t)} \int\int d\omega_1\, d\omega_2 [\omega_2 - \langle \omega(t)\rangle_{\mathrm{pr}}](\omega_1 - \langle \omega\rangle_{pu}) \times W(\omega_2|E_{pr}) P(\omega_2;t|\omega_1) W(\omega_1|E_{pu}) \sigma_{\mathrm{abs}}(\omega_1), \quad (1)$$

where $\sigma_{\rm abs}$ is the distribution function for the transition energy (absorption spectrum) in the equilibrium ground electronic state and $W(\omega|E)$ is a filtering function for the electric field E. $P(\omega_2;t|\omega_1)$ is the conditional probability in the ground electronic state that the transition energy of the system is ω_2 at time t when the system was initially prepared with a transition energy of ω_1. As Kinoshita has discussed, a stochastic evolution of transition energy is justified based on the random occupation of phonon states (inhomogeneous broadening) via the thermal energy.[22] However, by the definition of the conditional probability, ω_1 and ω_2 in Eq. (1) should be identical at time zero, that is, $P(\omega_2,0;\omega_1)=\delta(\omega_1-\omega_2)$. Clearly this approach excludes the possibility of homogeneous broadening (as defined above) and hence cannot explain the zero difference peak shift at short times. The function $N(t)$ describes the total population transfer kinetics from the pump to probe regions (interband population transfer) illustrated by panel (a) of Fig. 10 when the dynamics of spectral evolution is described by the given conditional probability, $P(\omega_2;t|\omega_1)$:

$$N(t)\equiv\int_{-\infty}^{\infty}d\omega_1\int_{-\infty}^{\infty}d\omega_2\,W(\omega_2|E_{pr})\times P(\omega_2;t|\omega_1)W(\omega_1|E_{pu})\sigma_{\rm abs}(\omega_1). \tag{2}$$

Then Eq. (1) is a time-correlation function of the transition energy (normalized by a time-dependent spectral population), which measures the portion of the ensemble retaining memory of its transition energy (the probability of interband memory transfer) illustrated by panel (b) of Fig. 10. $\langle\omega\rangle_{pu}$ and $\langle\omega(t)\rangle_{pr}$ are the mean frequencies of the systems pumped initially and probed at time t, respectively, which are given by

$$\langle\omega\rangle_{pu}=\frac{\int d\omega\,\omega W(\omega|E_{pu})\sigma_{\rm abs}(\omega)}{\int d\omega\,W(\omega|E_{pu})\sigma_{\rm abs}(\omega)}, \tag{3}$$

$$\langle\omega(t)\rangle_{pr}=N^{-1}(t)\int d\omega_1\int d\omega_2\,\omega_2\times W(\omega_2|E_{pr})P(\omega_2;t|\omega_1)W(\omega_1|E_{pu})\sigma_{\rm abs}(\omega_1). \tag{4}$$

An expression for the conditional probability has been derived by other groups[22–25] as

$$P(\omega_2;t|\omega_1)=\frac{1}{\sqrt{2\pi\Delta^2(1-M(t)^2)}}\times\exp\left(-\frac{[(\omega_2-\langle\omega\rangle)-(\omega_1-\langle\omega\rangle)M(t)]^2}{2\Delta^2[1-M(t)^2]}\right), \tag{5}$$

where Δ^2 ($\equiv\langle\delta\omega(0)^2\rangle$) is the coupling strength and is related to the reorganization energy via the relationship, $\Delta^2=2\lambda kT$, and $\langle\omega\rangle$ is the ensemble average value of the transition frequency in the equilibrium ground state.

In Fig. 11, we compare the simulated difference peak shift data and the correlation function, as given in Eq. (1). This figure confirms that the two-color difference peak shift follows the correlation function of the transition energies at the pump and probe regions, Eq. (1), except for early times. At these times, the population transferred from the pump to probe regions by the fluctuation of the inhomogeneous distribution is negligible, and only the homogeneous broadening mechanism that gives rise to a FID signal (as discussed above) contributes. Therefore the correlation function (1), which describes the memory transfer associated with the spectral shift, and the difference peak shift should not be compared at very short times. The reason that Eq. (1) gives higher values of rephasing capability at short times may arise from the fact that the conditional probability assumes a strong correlation between the initial and final frequencies and thus neglects the homogeneous broadening. After this transient period, fluctuations of the statistical distribution (inhomogeneous broadening) cause transfer of the initially excited population from the pump region, and the magnitude of this fluctuation dominates the homogeneous broadening mechanism, which is responsible for the FID signal. As a result, the rephasing capability of the total signal is well characterized by the correlation function (1). Equation (1), except for short times, qualitatively predicts the features of numerical simulations of the difference peak shift for different choices of the reorganization energy, the time scale of the Gaussian component, and the energy separation between the two pulses.

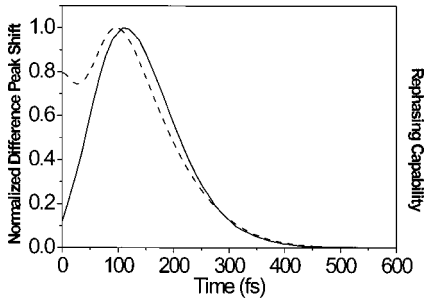

FIG. 11. A comparison of the results of a numerical simulation of the difference peak shift (solid line) with the model for rephasing capability described by Eq. (1) (dashed line). The $M(t)$ consists of a single Gaussian mode ($\lambda=600\ {\rm cm}^{-1}$; $\tau_g=200$ fs). Equation (1) reproduces all the features of the numerical simulation qualitatively after a certain transient time. All the curves are normalized for a direct comparison.

This argument implies that the total response function can be thought of as approximately the sum of two contributions whose amplitudes, $P_{\rm inhom}(t)$ and $P_{\rm hom}(t)$, are time dependent,

$$R(t;\omega_{pr},\omega_{pu})=P_{\rm inhom}(t)R_{\rm inhom}(t)+P_{\rm hom}(t)R_{\rm hom}(t). \tag{6}$$

Of course, it is not possible to rigorously separate out the response function into the two additive contributions. Similarly the total time correlation function characterizing the signal can be modeled as

$$\langle\delta\epsilon_{pr}(t)\,\delta\epsilon_{pu}\rangle=\frac{P_{\rm inhom}(t)}{P_{\rm inhom}(t)+P_{\rm hom}(t)}\langle\delta\epsilon_{pr}(t)\,\delta\epsilon_{pu}\rangle_{\rm inhom}+\frac{P_{\rm hom}(t)}{P_{\rm inhom}(t)+P_{\rm hom}(t)}\langle\delta\epsilon_{pr}(t)\,\delta\epsilon_{pu}\rangle_{\rm hom}. \tag{7}$$

The first term is the correlation function, Eq. (1), associated with the fluctuation of inhomogeneous distribution weighted by the relative contribution of the fluctuation. The second term is the correlation function associated with the homogeneous distribution. For low-frequency solvation modes, $P_{\mathrm{hom}}(t)$ is expected to be quite small. Therefore, except at a very short time before $P_{\mathrm{inhom}}(t)$, is developed, the contribution of the second term of Eq. (7) will be negligible. In this picture the reason why Eq. (1) deviates from the full calculation at short times is because the contribution from the first term in Eq. (7) is very small initially. At present, we do not have a model to describe the detailed behavior of $P_{\mathrm{inhom}}(t)$ and $P_{\mathrm{hom}}(t)$, but Eq. (7) seems to provide an adequate physical picture of the rise and decay of the difference peak shift.

To summarize, at short times there are no common transitions between the pump and probe pulses and the system has no rephasing capability. As the system evolves, solvent molecules undergo motion, causing fluctuations in the electronic transition energy and also the Stokes shift. The memory of the initially created nuclear states is then transferred to other parts of the spectrum that are probed by the final pulse. In other words, the new nuclear states resulting from solvent dynamics retain partial memory of the initially created states. This leads to an increased contribution from the echo signal and increases the difference peak shift. As the system evolves further, diffusional relaxation occurs, causing changes in the liquid structure[26] that lead to a decay in the difference peak shift.

Such a picture clearly suggests a distinction between the downhill and uphill difference peak shift in a system undergoing a systematic red shift. Furthermore, in a system with many vibronic transitions there appears to be an interference between the solvent fluctuations and the vibrational wave packet oscillations and dephasing such that the sensitivity of the uphill difference peak shift to the ultrafast solvation process is almost eliminated. The question immediately arises as to why the simulated downhill difference peak shift seems rather insensitive to vibrational effects. We do not, as yet, have a microscopic answer to this question, but it may lie in a time scale separation between the dephasing of the many sum and difference frequencies created by pulses 1 and 2,[16,27] and the time scale of the Stokes shift. In any case a reasonable model for the solvation dynamics allows us to fit the difference peak shift for IR144 in methanol quite well (Fig. 12). The $M(t)$ is the same as discussed in the context of Fig. 8, except that the Gaussian time constant used was 220 fs. Note that this value is significantly longer than that estimated previously from the one-color peak shift[3] and 2-D experiments.[12,13] In Fig. 12 we have also shown the difference peak shift obtained using a Gaussian time constant of 120 fs, and it reaches a maximum value much earlier than the experimental data. For IR144 in methanol, the presence of a large number of intramolecular modes with significant coupling strength makes the one-color peak shift data not very sensitive to the Gaussian time constant. The turnover behavior of the difference peak shift, appears to allow a more reliable estimate of the Gaussian time constant. We should point out that our results are not specific to a particular solute–solvent system. We have carried out experiments on

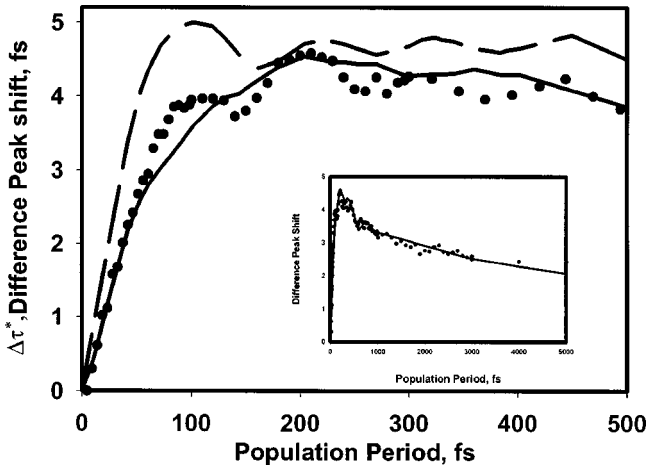

FIG. 12. A comparison of the downhill (750–750–800 nm) difference peak shift for IR144 in methanol with the numerical simulations. The parameters are the same as described in Fig. 8 with the Gaussian time constant set at 220 fs (solid line). The inset shows the same data and simulation for a longer population period. Also shown is the difference peak shift simulation performed with a 120 fs Gaussian component while keeping all the other parameters fixed (dashed line).

IR144 and on DTTCI in several solvents and in all cases the difference peak shift starts at a near zero value and increases to a maximum on an ultrafast time scale. The downhill difference peak shift of DTTCI in methanol also suggests that the Gaussian time constant is ~240 fs and is in agreement with the results of de Boeij *et al.*[7] and Lee *et al.*[28] We have generally observed that the simulations are in better agreement with the difference peak shift values than with the type I and II peak shifts individually. We believe that this is due to a partial cancellation of the finite pulse duration effect and the influence of the intramolecular modes on the difference peak shift than in the type I and II peak shifts separately. It is usually very hard to account for all the intramolecular modes in the calculation of the signal, as not much is known about the frequencies of the modes and their coupling strengths to the electronic transition.

Solvation time correlation functions (TCF) obtained from molecular dynamics simulations for an atomic solute in methanol give inertial timescales of ~100 fs.[29,30] The TCF also generally shows oscillations with a period of 20–30 fs. This oscillation was attributed to the libration of the OH group, and the 100 fs component was assigned to the inertial motion along the two other (nearly degenerate, but larger) moments of inertia components in the C–OH plane.[30] The 100 fs initial decay component, however, increases appreciably if the solute size is increased (20%–30% depending on the electrostatic nature of the solute) to accord with the type of dye molecules used experimentally,[30–32] or the order of the multipole interaction responsible for the fluctuations increase.[30] The initial time scale of the solvent response was also found to increase if the polarizability of the solute is taken into account.[30,33–35] The slowing of the solvent response with increasing solute polarizability was attributed (in part) to the change in the solvation force constant due to the rapid response of the dipole moment of the solute in response to an environmental (solvent) polarization fluctuation.

Given these three factors a value of 220 fs does not seem unreasonable for the ultrafast solvation timescale of IR144 in methanol.

The notion that 2C3PEPS is sensitive to the degree of correlation of transition frequency between initial and final states raises the prospect of many interesting studies of dynamics. As a specific example, consider incoherent energy transfer via the Forster mechanism between donor and acceptor pairs in an inhomogeneous ensemble, such as exists, for example, in Photosystem I of green plants and cynobacteria.[36] As we showed previously, even though donor–acceptor pairs are distributed randomly in transition frequency, larger rates between those pairs with good spectral overlap lead to the partial correlation of donors and acceptors.[37] A simple calculation based on this model shows that such an energy transfer-induced correlation appears as a rise in the two-color difference peak shift signal. Such studies then could be attractive for characterizing the nature of both diagonal and off-diagonal disorder in natural and synthetic antenna systems.

The asymmetrical influence of vibrational degrees of freedom to the uphill and downhill peak shifts is intriguing. The same model that describes the downhill difference peak shift fairly well produces a relatively poor agreement for the oscillatory component with the experimental uphill difference peak shift (figure not shown). We suspect that the two-color experiments will require a significant improvement in the description of vibrational dynamics to provide accurate amplitudes and phases of vibrational modulations as various points on the potential surface are accessed.

To sum up, we have described a new variant of the photon echo peak shift, which, by projecting out events in which an individual molecule interacts with light fields at two different frequencies, is capable of providing novel insights into molecular dynamics. A key quantity is the difference peak shift, which minimizes the effects of finite pulse duration and projects out the rephasing capability at the frequency of the third pulse. While analytical expressions for the difference peak shift remain to be derived, our numerical modeling suggests that the two-color difference peak shift will be of interest for studies of correlations between reactant and product states in a variety of contexts. For example, experiments in which a substantial portion of the potential surface is probed by systematic variation of the frequency of pump and probe frequencies may allow accurate investigations of the validity of linear response in polar,[30,31,38–42] and nonpolar solvation dynamics.[42] A recent theoretical study by Matyushov[43] showed that the Stokes-shift correlation function is insensitive to the nonlinear solute–solvent effects, whereas the change in spectral shape is more sensitive to such effects. Since the two-color photon echo technique probes different parts of the potential, it should be more sensitive to the shape of the spectrum, and thus the actual solute–solvent potential. The technique may then be useful to study nonlinear solvation dynamics.

ACKNOWLEDGMENTS

The authors thank Mark Maroncelli for his insights into solvation dynamics in methanol. This work was supported by a grant from the National Science Foundation (NSF), and in part by the Director, Office of Science, Office of Basic Energy Sciences, Chemical Sciences Division, of the U.S. Department of Energy under Contract No. DE-AC03-76SF00098.

[1] N. Morita, T. Tokizaki, and T. Yajima, J. Opt. Soc. Am. B **4**, 1269 (1987).
[2] A. M. Weiner, S. De Silvestri, and E. P. Ippen, J. Opt. Soc. Am. B **2**, 654 (1985).
[3] T. Joo, Y. Jia, J.-Y. Yu, M. J. Lang, and G. R. Fleming, J. Chem. Phys. **104**, 1 (1996).
[4] M. Cho, J.-Y. Yu, T. Joo, Y. Nagasawa, S. A. Passino, and G. R. Fleming, J. Phys. Chem. **100**, 11944 (1996).
[5] G. R. Fleming and M. Cho, Annu. Rev. Phys. Chem. **47**, 109 (1996).
[6] G. R. Fleming, T. Joo, and M. Cho, Adv. Chem. Phys. **101**, 141 (1997).
[7] W. de Boeij, M. S. Pshenichnikov, and D. A. Wiersma, J. Phys. Chem. **100**, 11806 (1996).
[8] M. S. Pshenichnikov, K. Duppen, and D. A. Wiersma, Phys. Rev. Lett. **74**, 674 (1995).
[9] P. Vöhringer, D. C. Arnett, T.-S. Yang, and N. F. Scherer, Chem. Phys. Lett. **237**, 387 (1995).
[10] W. P. de Boeij, M. S. Pshenichnikov, and D. A. Wiersma, Chem. Phys. Lett. **238**, 1 (1995).
[11] W. P. de Boeij, M. S. Pshenichnikov, and D. A. Wiersma, Chem. Phys. **233**, 287 (1988).
[12] J. D. Hybl, S. M. G. Faeder, A. W. Albrecht, C. A. Tolbert, D. C. Green, and D. M. Jonas, J. Lumin. **126**, 87 (2000).
[13] J. D. Hybl, A. A. Ferro, and D. M. Jonas, J. Chem. Phys. **115**, 6606 (2001).
[14] M. Yang and G. R. Fleming, J. Chem. Phys. **110**, 2983 (1999).
[15] S. Mukamel, *Principles of Nonlinear Optical Spectroscopy* (Oxford University Press, New York, 1995).
[16] K. Ohta, D. S. Larsen, M. Yang, and G. R. Fleming, J. Chem. Phys. **114**, 8020 (2001).
[17] R. M. Stratt, Acc. Chem. Res. **28**, 201 (1995).
[18] R. M. Stratt and M. Cho, J. Chem. Phys. **100**, 6700 (1994).
[19] M. Cho, G. R. Fleming, S. Saito, I. Ohmine, and R. M. Stratt, J. Chem. Phys. **100**, 6672 (1994).
[20] G. Garberoglio and R. Vallauri, J. Chem. Phys. **115**, 395 (2001).
[21] T. S. Kalbfleisch, L. D. Ziegler, and T. Keyes, J. Chem. Phys. **105**, 7034 (1996).
[22] S. Kinoshita, J. Chem. Phys. **91**, 5175 (1989).
[23] R. F. Loring, Y. J. Yan, and S. Mukamel, J. Chem. Phys. **87**, 5840 (1987).
[24] S. Mukamel, J. Chem. Phys. **79**, 2126 (1983).
[25] M. D. Stephens, J. G. Saven, and J. L. Skinner, J. Chem. Phys. **106**, 2129 (1997).
[26] E. F. David and R. M. Stratt, J. Chem. Phys. **109**, 1375 (1998).
[27] D. S. Larsen, K. Ohta, Q.-H. Xu, M. Cyrier, and G. R. Fleming, J. Chem. Phys. **114**, 8008 (2001).
[28] S.-H. Lee, J.-H. Lee, and T. Joo, J. Chem. Phys. **110**, 10969 (1999).
[29] M. Maroncelli, P. V. Kumar, A. Papazyan, M. L. Horng, S. J. Rosenthal, and G. R. Fleming, in *Proceedings of the International Workshop*, Ultrafast Reaction Dynamics and Solvent Effects (Abbaye de Royaumont, France, 1993).
[30] P. V. Kumar and M. Maroncelli, J. Chem. Phys. **103**, 3038 (1995).
[31] E. A. Carter and J. T. Hynes, J. Chem. Phys. **94**, 5961 (1991).
[32] H. L. Friedman, F. O. Raineri, F. Hirata, and B. C. Perng, J. Stat. Phys. **78**, 239 (1995).
[33] B. D. Busulaya, D. A. Zichi, and H. J. Kim, J. Phys. Chem. **99**, 10069 (1995).
[34] B. D. Busulaya, D. A. Zichi, and H. J. Kim, J. Phys. Chem. **100**, 1392 (1996).
[35] K. Ando, J. Chem. Phys. **107**, 4585 (1997).
[36] P. Jordan, P. Fromme, H. T. Witt, O. Klukas, W. Saenger, and N. Krauss, Nature (London) **411**, 909 (2001).
[37] M. Yang and G. R. Fleming, J. Chem. Phys. **113**, 2823 (2000).
[38] R. Olender and A. Nitzan, J. Chem. Phys. **102**, 7180 (1995).
[39] M. Maroncelli, J. Chem. Phys. **94**, 2084 (1991).
[40] T. Fonseca and B. M. Ladanyi, J. Phys. Chem. **95**, 2116 (1991).
[41] B. M. Ladanyi and R. M. Stratt, J. Phys. Chem. **100**, 1266 (1996).
[42] B. Ladanyi and M. Maroncelli, J. Chem. Phys. **109**, 3204 (1998).
[43] D. V. Matyushov, J. Chem. Phys. **115**, 8933 (2001).